Building Engineering 2025, 3(1), 1834.
https://doi.org/10.59400/be1834

Article

A comparative research of the Piloti-type RC structure and non-Piloti-type RC structure under the nonlinear pushover analysis

Mo Shi[1,2,*], Minwoo Choi[1], Yeol Choi[1]

[1] School of Architecture, Kyungpook National University, Daegu 41566, Korea
[2] HaXell Elevator Co., Ltd., Shanghai 201801, China
*** Corresponding author:** Mo Shi, shimo0204@outlook.jp

CITATION

Shi M, Choi M, Choi Y. A comparative research of the Piloti-type RC structure and non-Piloti-type RC structure under the nonlinear pushover analysis. Building Engineering. 2025; 3(1): 1834. https://doi.org/10.59400/be1834

ARTICLE INFO

Received: 8 October 2024
Accepted: 5 November 2024
Available online: 25 November 2024

Abstract: With the ongoing acceleration of the urbanization process, a large portion of the population is concentrated in urban areas, leading to significant issues with living space. The increasing number of vehicles necessitates more parking space, and the phenomenon of urbanization requires new building structures that can accommodate this need. As a result, there has been a rise in Piloti-type RC (reinforced concrete) structures, particularly in the Republic of Korea. These structures utilize their open ground floors for various purposes such as parking, storage, and social spaces, adding functional diversity to buildings and receiving positive reviews for these advantages. However, the open ground floor can potentially create security vulnerabilities if not adequately secured or monitored. This was evident during the Pohang earthquake in 2017 when numerous Piloti-type RC structures sustained more severe damage than conventional RC structures. Therefore, numerous previous researchers have emphasized the importance of ensuring structural safety in Piloti-type RC structures. In this research, the structural designs under the Ministry of Land, Infrastructure, and Transport of the Republic of Korea were used as a basis for simulation in SAP 2000. The focus was on comparing the structural performance of a typical Piloti-type RC structure with and without the Piloti-type design using nonlinear pushover analysis. The findings of this research are expected to provide a clear understanding of the differences between Piloti-type RC structures and non-Piloti-type RC structures. Additionally, based on the specific characteristics of Piloti-type RC structural vulnerabilities identified through nonlinear pushover analysis, this research is anticipated to serve as a valuable reference for reinforcing existing Piloti-type RC structures to better resist seismic activities, thereby reducing human casualties and economic damage resulting from seismic events.

Keywords: Piloti-type RC structure; nonlinear pushover analysis; seismic damage; structural simulation; SAP 2000

1. Introduction

Piloti-type RC (reinforced concrete) buildings are characterized by their elevated first floors, which are supported by columns with open spaces underneath. This structural style offers several practical and aesthetic benefits, making it popular in contemporary society for various types of buildings such as residential complexes, commercial buildings, and public spaces. The advantages of Piloti-type RC buildings, such as space utilization for parking and recreational areas, have made this type of structure very popular in the Republic of Korea. These buildings address many living issues, including parking problems due to the increasing number of vehicles. Additionally, they can be used for gardens, playgrounds, or communal spaces to enhance the quality of life for residents.

However, the research conducted by Jiuk et al. [1] indicates the structural issues related to Piloti-type RC buildings. Much previous research emphasizes concerns such as seismic considerations, including soft-story effects, mitigation measures, shear walls, bracing systems, and strong column-weak beam relationships. Additionally, load distribution and material quality have been identified as major aspects in previous research. Despite these considerations, many Piloti-type RC buildings exhibited structural weaknesses during the Pohang 2017 earthquake, as **Figure 1** illustrates. The ground floor columns of these buildings were particularly susceptible to damage due to their unique characteristics. This emphasizes the need for a thorough analysis of Piloti-type RC buildings and the development of effective seismic resistance methods.

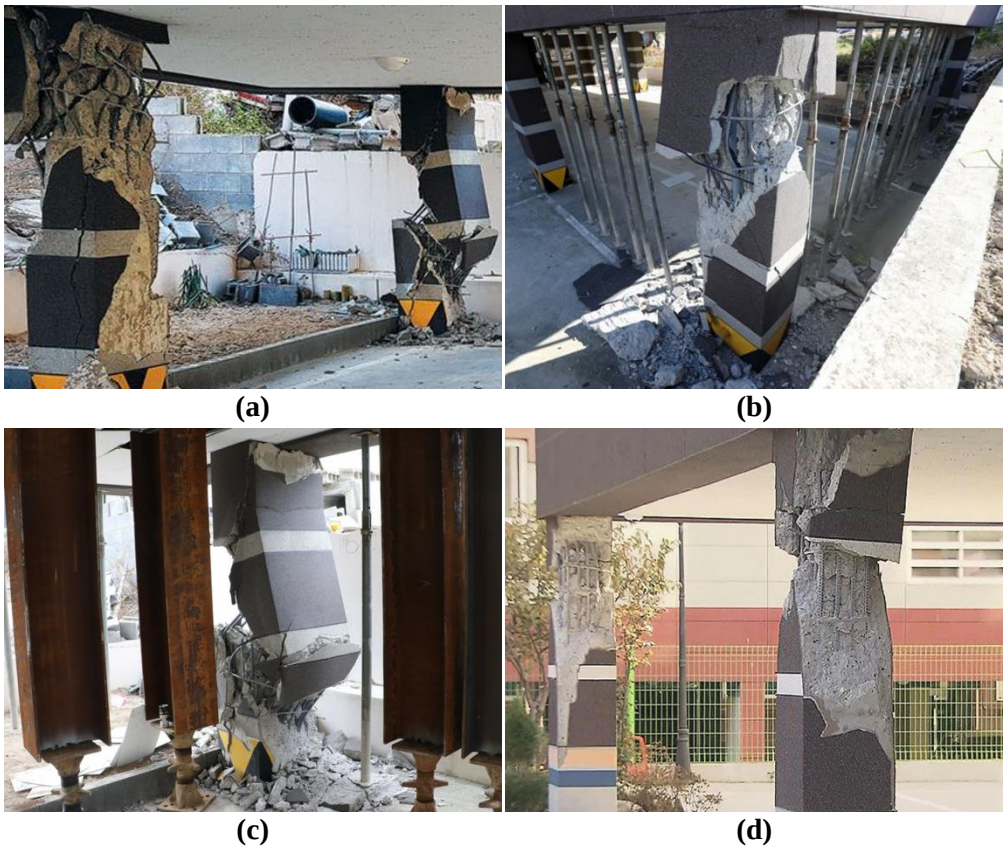

(a) **(b)**

(c) **(d)**

Figure 1. Damage of Piloti-type RC buildings. **(a)** Parking area; **(b)** opening space; **(c)** structural repairing; **(d)** school building.

As noted by Honda et al. [2], Piloti-type RC buildings offer numerous benefits such as efficient space utilization, modern aesthetics, and flood protection. However, based on the structural damages of Piloti-type RC buildings with the Pohang 2017 earthquake, it is essential that careful attention be given to the Piloti-type RC structural design in order to address potential seismic vulnerabilities and ensure safety and stability [3–8]. With proper engineering solutions in place, Piloti-type RC buildings can provide functional, yet attractive, resilient spaces within contemporary urban environments.

Although a lot of research has identified the vulnerability of ground floor columns in Piloti-type RC buildings, few have conducted detailed analytical comparisons between Piloti-type and non-Piloti-type RC structures within the same

structural framework [3–8]. The absence of such comparative research limits a full understanding of how open spaces on the ground floor affect mechanical performance and structural integrity. The comparison is expected to highlight the mechanical influence of the open spaces of Piloti-type structures, shedding light on the potential challenges that Piloti-type RC buildings face in seismic activities. Therefore, this research seeks to bridge that gap by systematically analyzing and contrasting the behavior of these two structural designs under nonlinear pushover analysis. By exploring the structural characteristics, this research provides critical insights into the strengths and weaknesses of Piloti-type RC buildings. Additionally, it offers a valuable reference for developing targeted reinforcement strategies to improve seismic resilience, ensuring that Piloti-type RC buildings can safely withstand external forces while maintaining the functional advantages of the Piloti-type RC buildings in urban environments.

In this research, a typical Piloti-type RC building provided by the Ministry of Land, Infrastructure, and Transport of the Republic of Korea was selected for simulation using nonlinear pushover analysis in SAP 2000. The response spectrum was based on the Pohang 2017 earthquake and selected according to the earthquake site of Pohang City, referring to the Korean Design Standard KDS 41 17 00: 2022 in order to determine performance points. Two different RC structures with and without Piloti-type designs were simulated based on the typical Piloti-type RC building. The comparative analytical results of base shear, structural lateral displacement, layer shear, and layer drift are expected to provide valuable references for newly built Piloti-type RC buildings. Additionally, this research is also expected to serve as a reference for reinforced projects for existing Piloti-type RC buildings in order to resist seismic damages while reducing human casualties and economic damage resulting from seismic activities.

2. Description of the research

2.1. Structural design

The floor plan design serves as a crucial tool for illustrating the design of the target Piloti-type RC building in this research, as shown in **Figure 2**. The target Piloti-type RC building is designed by the Ministry of Land, Infrastructure, and Transport of the Republic of Korea, with dimensions spanning 14.8 m in length and 13 m in breadth. As depicted in **Figure 2**, the area of the target Piloti-type RC building in this research can be calculated to be 192.4 m^2.

Figure 2 also indicates that a total of 16 columns are incorporated into the design of the target Piloti-type RC building, with two different column section designs labeled C1 and C2. Specifically, 14 columns are designated for structural general use (C1), while 2 columns are allocated for the core area (Stair Zone) using the column design of C2. Additionally, beam section S is connected to each column throughout the entire structure. Furthermore, two different wall sections labeled W1 and W2 are utilized for general structural designs and within the core area (Stair Zone) of the target Piloti-type RC building respectively.

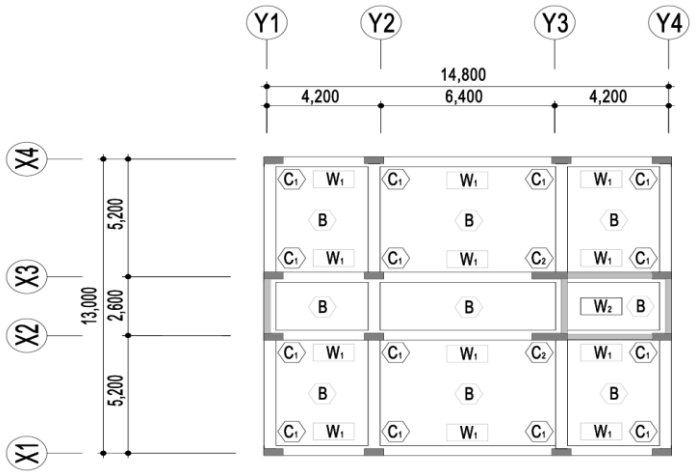

Figure 2. Design of the floor plan.

The structural elevation is a significant aspect of achieving the 3D model on SAP 2000. The structural elevation of the target Piloti-type structure in this research is showcased in **Figure 3**, providing a clear front view and side view. According to the structural elevation, the first floor with the Piloti-type structure design is planned with a height of 3.3 m, and each single story from the 2nd floor to the roof floor of the 5th floor is planned with a height of 2.7 m. Additionally, the stair zone in the core area on the roof in this target Piloti-type structure is planned with a height of 2.8 m. Based on these story height designs, the structural height of the building is given as 14.2m as illustrated in **Figure 3**.

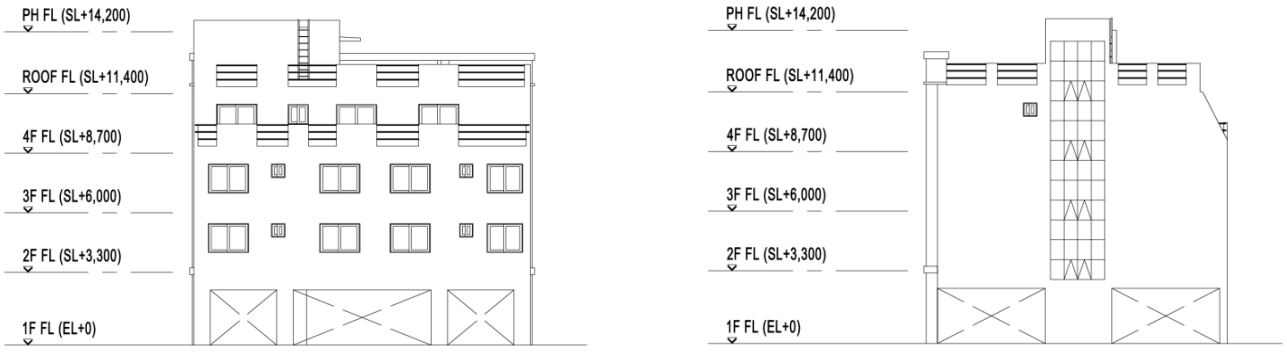

(a) **(b)**

Figure 3. Piloti-type structural elevation. **(a)** Front view; **(b)** side view.

Especially, this research has taken into account not only the material used for the reinforcement rebars but also the design definition of the cross-section of beam and columns as the subsequent section 2.2 illustrates. Both of these factors are crucial in determining the appropriate amount and strength of the rebars required for the structural integrity of the design. This research has ensured that the reinforcement rebars used align precisely with the actual structural design specifications, which is a vital aspect for the accuracy and reliability under the nonlinear pushover analysis in this research. The detailed illustration of how the material and cross-section of beam and columns design definition along with the amount and strength of reinforcement

rebars correspond with the actual structural design is provided in the subsequent section, labeled as section 2.2.

2.2. Material property and section designs

Since concrete is the primary material used in the construction of the target Piloti-type RC structure in this research, the material properties of the concrete have a significant impact on the results under the nonlinear pushover analysis conducted in this research. The properties of concrete are defined according to the Korean Standard KS F 4009: 2021 (Ready-mixed concrete), as presented in **Table 1**. The concrete utilized in the target Piloti-type RC structure in this research complies with Korean national industry standards for consistency, durability, and performance.

Table 1. Concrete property.

Weight per unit volume	25,000 N/m^3
Mass per unit volume	2550 kg/m^3
Modulus of Elasticity (E)	30,000 MPa
Poisson (U)	0.18
Coefficient of Thermal Expansion (A)	1.000E-05
Shear Modulus (G)	12,500 MPa
Specified Compressive Strength (F_{ck})	21 MPa
Expected Compressive Strength (F_{ek})	26.25 MPa

According to the Korean Standard KS F 4009: 2021 (Ready-mixed concrete), as shown in **Table 1**, the specified compressive strength of the concrete is indicated as F_{ck} = 21 MPa. After applying a multiplication coefficient of 1.2, the expected compressive strength of the concrete denoted as F_{ek} = 25.2 MPa, provides insight into its potential performance under real-world conditions. This takes into account factors such as curing time, environmental influences, and quality control measures.

In addition, the weight per unit volume of the concrete is specified as 25,000 N/m^3, while the mass per unit volume is given as 2550 kg/m^3. The Poisson ratio for defining the concrete properties in this research is determined to be 0.18 as **Table 1** illustrates.

Table 2. Rebar property.

Weight per unit volume	77,000 N/m^3
Mass per unit volume	7850 kg/m^3
Modulus of Elasticity (E)	200,000 MPa
Poisson (U)	0.3
Coefficient of Thermal Expansion (A)	1.170E-05
Minimum Yield Stress (F_y)	400 MPa
Minimum Tensile Stress (F_u)	540 MPa
Expected Yield Stress (F_{ey})	440 MPa
Expected Tensile Stress (F_{eu})	590 MPa

The material property of the rebar is also a key aspect of the target Piloti-type RC structure in this research. The rebar property is defined according to the Korean standard KS D 3504: 2021 (Steel bars for concrete reinforcement), as shown in **Table 2**. Specifically, the yield strength of the rebar is designated as F_y = 400 MPa, and the expected yield stress of the rebar is designated as F_{ey} = 440 MPa. These values provide valuable parameters for evaluating the expected performance of the rebar under nonlinear pushover analysis in this research.

Furthermore, as illustrated in **Table 2**, the weight per unit volume of the rebar in this research is specified as 77,000 N/m^3, while the mass per unit volume is given as 7850 kg/m^3. The Poisson ratio for defining the rebar properties in this research is determined to be 0.3.

The nonlinear behavior of concrete and rebar plays a critical role in the nonlinear pushover analysis conducted in this research. Given the importance of capturing the accurate mechanical responses of materials under load, this research leverages detailed material specifications presented in **Tables 1** and **2**, which provide essential parameters for concrete and rebar, and these parameters establish an accurate framework for analyzing structural response to increasing loads.

In addition, **Figure 4** graphically represents the nonlinear properties of the materials as concrete and rebar, with **Figure 4a** showing the stress-strain curve for concrete and **Figure 4b** depicting the stress-strain curve for rebar. By incorporating these nonlinear material properties, the analysis accurately reflects how each component contributes to the overall structural performance under simulated seismic conditions. This approach not only ensures realistic modeling but also improves the reliability of the results, establishing a robust foundation for evaluating structural safety and resilience in RC structures under the nonlinear pushover analysis.

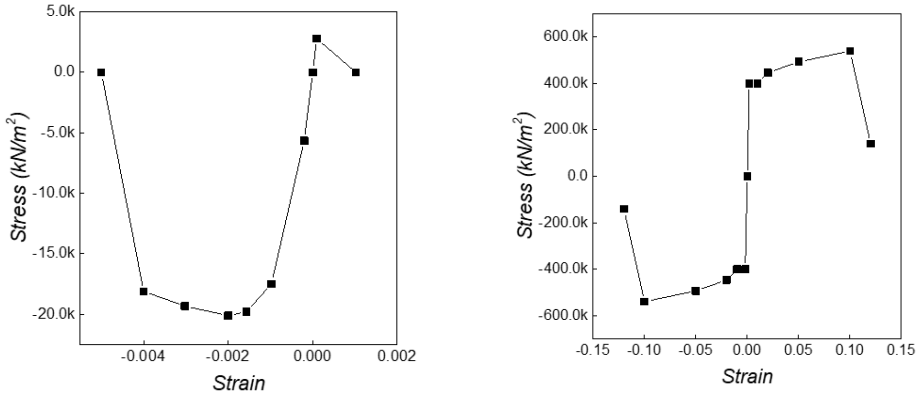

(a) **(b)**

Figure 4. Nonlinear property of concrete and rebar. **(a)** Concrete; **(b)** Rebar.

Including considerations for structural integrity, load transfer, and resistance to lateral forces, columns are vertical structural elements that play a crucial role in supporting the weight of the building and safely transferring it to the foundation. In this research, the column plays a significant role in the target Piloti-type RC structure. Two different column sections, named C1 and C2 as illustrated in **Figure 5**, are defined for further analysis.

Figure 5. Column section designs. **(a)** Section design C1; **(b)** section design C2.

Referring to **Figure 5a**, column section C1 is designed for general column utilization in the target Piloti-type RC structure, with a cross-sectional area of 210,000 mm^2 and dimensions of 700 mm × 300 mm. Within the C1 section, reinforcing rebars are arranged to enhance structural robustness and resilience. Specifically, ten longitudinal D22 (Diameter: 22 mm) rebars are positioned within the C1 section, complemented by D10 (Diameter: 10 mm) hoop rebars spaced at intervals of 150 mm. Furthermore, according to the Korean Standards outlined in KDS 14 20 50: 2022, a regulatory framework dictates a concrete covering depth of 40 mm for the general RC structures.

On the other hand, in **Figure 5b**, column section C2 is specifically designed for the column located in the core area (Stair zone) of the Piloti-type RC structure under consideration. It has a cross-sectional area of 390,000 mm^2 and dimensions of 1300 mm × 300 mm. Within section C2, reinforcing rebars are also designed to enhance structural robustness and resilience. More precisely, fourteen longitudinal D22 (Diameter: 22 mm) rebars are positioned within section C2, accompanied by D10 (Diameter: 10 mm) hoop rebars spaced at intervals of 150 mm. Similar to the column section design of C1, in accordance with Korean Standard KDS 14 20 50: 2022, a construction code also dictates a concrete covering depth of 40 mm for the column design of C2.

Similar to the column section, which includes considerations such as structural support, span capability, and resistance to deflection, the significance of beams in RC structures is vast and multifaceted. In this study, the beam section is designed with a consistent unified approach, as illustrated in **Figure 6**.

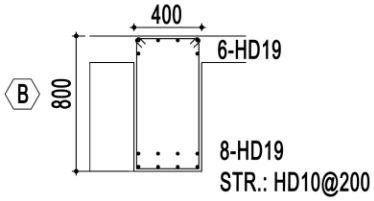

Figure 6. Beam section design.

In accordance with **Figure 6**, the beam section of the target Piloti-type RC structure is designed with a unified design, featuring a cross-sectional area of 320,000 mm^2 and dimensions of 400 mm × 800 mm. Similar to the column section designs, the reinforcing rebars are also positioned to enhance the structural robustness and resilience of the beam section. Specifically, six longitudinal D19 (Diameter: 19 mm) rebars are located on the top of the beam section (Compression Zone), while eight longitudinal D19 (Diameter: 19 mm) rebars are placed on the bottom of the beam section (Tensile Zone). Additionally, D10 (Diameter: 10 mm) hoop rebars are spaced

at intervals of 200 mm to further reinforce the beam section. Moreover, it should be noted that according to Korean Standard KDS 14-20-50: 2022, the concrete covering depth of 40 mm is designed for the beam section also.

The slab in the RC structure plays a crucial role, significantly contributing to the overall strength, stability, and functionality of the construction. The design of the slab for the target Piloti-type RC structure is depicted in **Figure 7** in this research.

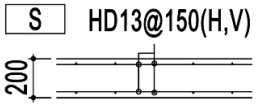

Figure 7. Slab design.

Referring to **Figure 7**, the slab design includes a total section thickness of 200 mm. According to the Korean Standard KDS 14 20 50: 2022, this involves a concrete cover of 40 mm. As shown in **Figure 7**, the rebar with D13 specifications (Diameter: 13 mm) is arranged in a grid pattern with two layers at both the top and bottom at angles of 0º and 90º, along with hoop rebars spaced at intervals of 150 mm, also with D13 specifications (Diameter:13 mm).

The wall system in the context of RC structures refers to a vertical element that provides stability, and strength, and sometimes serves as a barrier. The wall is significant to the target Piloti-type RC structure as it serves as the vertical element in this research. **Figure 8** illustrates two different designs of the wall system.

Figure 8. Wall designs. **(a)** Wall design W1; **(b)** Wall design W2.

Referring to **Figure 8a**, the wall system of W1 is designed for general utilization in the target Piloti-type RC structure and has a total section thickness of 200 mm. The reinforcing rebars within the W1 wall system are strategically arranged to enhance structural robustness and resilience. Specifically, rebars with D13 specifications (Diameter: 13 mm) are arranged in a grid pattern with two layers at both the top and bottom, positioned at angles of 0º and 90º, with rebars spaced at intervals of 150 mm.

On the other hand, in reference to **Figure 8b**, the wall system of W2 is specifically designed for the core area (stair zone) within the designated Piloti-type RC structure and features a thicker section thickness of 250 mm. Additionally, the reinforcing rebars within the W2 wall system are also arranged to enhance structural robustness and resilience. Similar to the design of the W1 wall system, rebars with D13 specifications (Diameter: 13 mm) are arranged in a grid pattern with two layers at both the top and bottom, positioned at angles of 0º and 90º, with rebars spaced at intervals of 150 mm. Furthermore, in accordance with the Korean Standard KDS 14 20 50: 2022, the concrete covering depth is consistently designed as 40 mm for both of the different wall system designs.

2.3. Load design and plastic hinges definition

Referring to the research conducted by Shi et al. [9], it is indicated that in the context of nonlinear pushover analysis, dead load and live load designs pertain to the various types of loads considered when evaluating the structural performance of the RC buildings under seismic or other dynamic loading conditions.

Regarding the nonlinear pushover analysis in this research, dead load plays a critical role in determining the overall structural behavior, as it directly contributes to the initial stiffness and strength of the structure [10–13]. This load primarily influences how the structure responds to lateral forces, such as those generated by seismic activities, ensuring stability during the early stages of deformation. Moreover, live load is not as impactful as dead load but remains a significant factor for realistic performance assessments in this research under the nonlinear pushover analysis [10–15].

In alignment with the Korean Standard KDS 41 10 15: 2019, Table 3.2-1 provides detailed guidelines for dead and live loads specific to residential structures. For the Piloti-type RC structure examined in this study, the dead load is assigned a value of 7.0 kN/m^2. This value reflects the static weight that the structure continuously carries, influencing the stiffness and initial strength of the structure for the nonlinear pushover analysis in this research. Meanwhile, the live load for the same structure is set at 5.0 kN/m^2, representing the variable loads resulting from the intended use and occupancy. While live load is not as critical as dead load for determining the inherent stiffness of the structure, it is essential for assessing the performance of the structure under the nonlinear pushover analysis.

In nonlinear pushover analysis, both the dead load and live load are typically included in the initial loading condition of the structural model. The analysis then proceeds by applying a monotonically increasing lateral load (e.g., seismic force) to the structure, simulating the effects of an earthquake or other dynamic event [16–18]. As the lateral load increases, the structure deforms and enters the inelastic range, ultimately reaching a point of failure or collapse. The capacity curve, which plots the base shear versus roof displacement, is used to assess structural performance. The capacity curve mainly provides valuable results about structural capacity, ductility, and overall response to lateral loading.

In the field of nonlinear pushover analysis, the consideration of load combinations plays a critical role in influencing structural assessment. The Korean Standard of KISTEC 2021 emphasizes the significance of load combinations in structural analyses and provides a calculated method to determine appropriate combinations of loads as the equation below:

$$LC = 1.0 \times DL + 0.25 \times LL \quad (1)$$

where *LC* is load combinations, *DL* indicates dead load and *LL* indicates live load.

In order to satisfy the specific simulation requirements for nonlinear pushover analysis, it is critical to assign plastic hinge properties to each structural component within the specific Piloti-type RC structure. The plastic hinges simulate the points of potential failure or yielding in the structure, where plastic deformations may occur as the structure experiences increasing external forces. The process of assigning these

plastic hinge properties is governed by the guidelines set out in the ASCE 41-13 standard, which provides detailed criteria for determining the necessary characteristics of the hinges [19–24]. Moreover, the ASCE 41-13 standard is fully supported by SAP 2000, which ensures that the simulation is not only accurate but also consistent with industry practices.

The plastic hinge representation for the column section in this research is defined following the guidelines set by the ASCE 41-13 standards. Specifically, the design of the plastic hinges follows the parameters and criteria outlined in Table 10-8 (modeling parameters and numerical acceptance criteria for nonlinear procedures—reinforced concrete columns) of the ASCE 41-13 standard. In this research, the plastic hinges for the columns are designed to address Condition ii-Flexure/Shear, a critical consideration for columns subjected to both bending and shear forces. The definitions of the hinges involve accounting for multiple degrees of freedom, which encompass axial forces, as well as bending moments along the M2 and M3 axes.

Specifically, regarding the column of C1, these properties are specifically characterized by axial forces, with the values assigned to the bending moments along the M2 and M3 axes. The bending moment values for column C1 are 1688.4 kN·m for the M2 axis and 422.1 kN·m for the M3 axis, highlighting the force distribution and the capacity of the column to withstand bending in different planes. Similarly, for column C2, the plastic hinge properties are also determined by axial forces, though with higher values compared to C1 based on the section design of C2. The bending moment values for column C2 are set at 3135.6 kN·m for the M2 axis and 783.9 kN·m for the M3 axis. These values indicate that column C2 has a greater capacity for resisting bending moments along both axes, reflecting its enhanced structural stiffness and strength.

By defining the plastic hinge properties, the analysis ensures that the nonlinear behavior of each column section is well-represented under nonlinear pushover analysis. The parameters are critical for assessing the overall performance of the Piloti-type RC structure in this research, allowing for modeling of how each column will react under the external load. The detailed characterization of bending moments for both C1 and C2 underscores the importance of understanding the unique behavior of different structural components within the Piloti-type RC structure, ultimately contributing to the effectiveness of the nonlinear pushover analysis.

The plastic hinge states, as defined by the ASCE 41-13 standard, play a critical role in evaluating the performance of RC structures, particularly when they enter the plastic zone. These hinge states are categorized into three key performance levels: IO (immediate occupancy), LS (life safety), and CP (collapse prevention). IO reflects a condition where the structure has experienced minimal post-earthquake damage and remains functional, with limited structural harm, LS indicates that while significant damage has occurred, there is still enough structural integrity to prevent partial or total collapse, ensuring the safety of occupants, and CP represents a severe damage state, where the building is on the verge of either partial or total collapse.

To further elaborate, the plastic hinge properties of columns C1 and C2 are outlined based on bending moments along the M2 and M3 axes. For column C1 as **Table 3** illustrates, the M2 axis values are as IO is set at 1693.47 kN·m, LS at 1703.60 kN·m, and CP at 1705.28 kN·m. For the M3 axis of column C1, IO is defined at 424.21

kN·m, LS at 441.09 kN·m, and CP at 447.43 kN·m. For column C2 as **Table 4** illustrates, the plastic hinge properties for the M2 axis are higher, reflecting its larger structural capacity as IO is set at 3145.01 kN·m, LS at 3163.82 kN·m, and CP at 3166.96 kN·m. Similarly, for the M3 axis of column C2, IO is 787.82 kN·m, LS at 819.18 kN·m, and CP at 830.93 kN·m.

Table 3. Plastic hinges on column C1.

Acceptance Criteria	Yield Moment	Coefficient	M2	Yield Moment	Coefficient	M3
	kN·m		kN·m	kN·m		kN·m
IO	1688.4	0.003	1693.47	422.1	0.005	424.21
LS	1688.4	0.009	1703.60	422.1	0.045	441.09
CP	1688.4	0.010	1705.28	422.1	0.060	447.43

Table 4. Plastic hinges on column C2.

Acceptance Criteria	Yield Moment	Coefficient	M2	Yield Moment	Coefficient	M3
	kN·m		kN·m	kN·m		kN·m
IO	3135.6	0.003	3145.01	783.9	0.005	787.82
LS	3135.6	0.009	3163.82	783.9	0.045	819.18
CP	3135.6	0.010	3166.96	783.9	0.060	830.93

The analysis of plastic hinge properties for columns C1 and C2 is essential for understanding the response under stress spanning from the elastic zone to collapse. **Figure 9** offers a detailed view of the properties that highlight how each column behaves across this spectrum. In particular, column C2 exhibits a notably higher yield moment than column C1 for both M2 and M3 moments, a difference attributable to the column section design as shown in **Figure 5**.

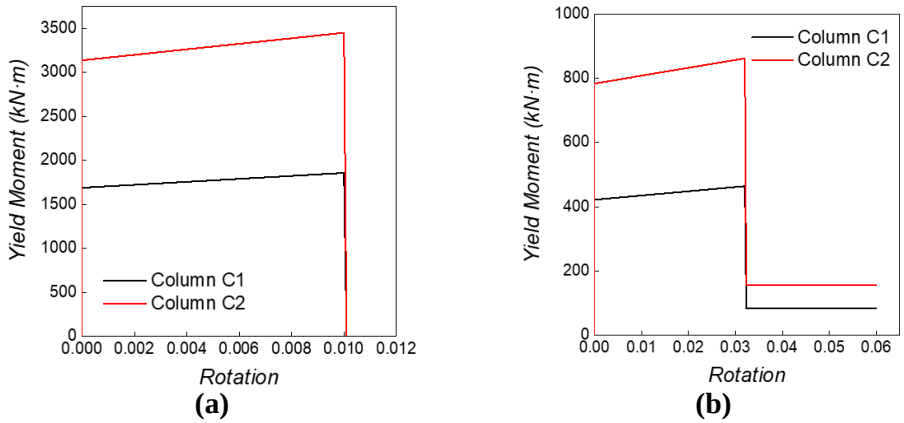

Figure 9. Plastic hinges properties of columns. **(a)** Column M2; **(b)** Column M3.

Figure 9a illustrates the higher yield moment for M2, where the design of column C2 enables it to sustain greater loads before yielding compared to column C1. Likewise, **Figure 9b** further underscores superior yield performance in M3 of column C2. The trend in **Figure 9** is also verified by values in **Tables 3** and **4**, which consistently show that the yield moment for M2 surpasses that of M3.

The plastic hinge modeling for beam sections in this research is also designed following the ASCE 41-13 standard. The guidelines governing this process are clearly outlined in Table 10-7, which serves as a critical resource for understanding the behavior of reinforced concrete beams during nonlinear static analysis procedures. An analytical point is designed for the M3 degree of freedom, which plays a vital role in assessing the performance of the beam, particularly in response to lateral forces and deformations that arise during seismic events or external pressures.

The plastic hinges for the beam section in this research are specifically designed with a yield moment of 307.97 kN·m, a critical value that signifies the point where the beam section starts to yield. The yield moment is a key factor in understanding how the structure will behave under applied loads. When this threshold is reached, the beam transitions from an elastic to a plastic state, meaning that permanent deformations begin to occur.

For a more comprehensive understanding of the performance of the beam under stress, **Table 5** offers detailed definitions of the plastic hinge properties, particularly focusing on yield moments across various structural performance levels—IO (immediate occupancy), LS (life safety), and CP (collapse prevention).

Table 5. Plastic hinges on beam.

Acceptance Criteria	Yield Moment	Coefficient	M3
	kN·m		kN·m
IO	307.97	0.01	311.05
LS	307.97	0.025	315.67
CP	307.97	0.05	323.37

At the IO level, the yield moment is recorded at 311.05 kN·m, which reflects the point at which the beam first experiences yielding with minimal structural damage. In this state, the structure remains functional, even after an event such as a moderate earthquake, highlighting the beam's ability to resist early-stage damage. As the beam endures further stress, the LS level shows a yield moment of 315.67 kN·m. At this stage, the structure sustains significant damage, but there is still a margin of safety against collapse, ensuring the protection of occupants even under more intense seismic activity. At the critical CP stage, the yield moment is measured at 323.37 kN·m, marking the beam's maximum capacity to withstand extreme stress without collapsing. This state represents the most severe level of damage that the beam can endure while still preventing a total structural failure.

Excepted the plastic hinge property of the beam on the plastic zone, **Figure 10** offers a comprehensive property of the plastic hinge behavior of the beam following the progression from the elastic zone all the way to collapse. **Figure 10** illustrates the yield moment of the beam which showcases both positive and negative values. The symmetric maximum yield moment values of the beam allow the resistance of both upward and downward forces. Referring to **Table 5** as the plastic hinge property in the plastic zone, **Figure 10** also reflects the plastic hinge properties in the plastic zone.

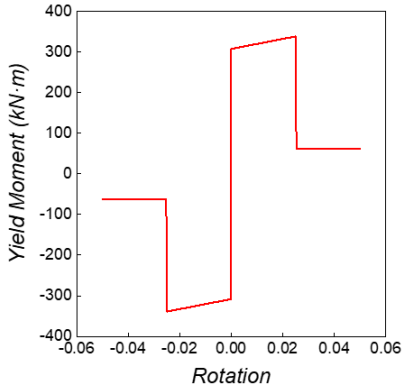

Figure 10. Plastic hinges properties of beam.

The analytical framework for the nonlinear pushover analysis in this research follows a systematic approach, with the load directions defined along two axes as *x* and *y*. These directions are essential for evaluating the structural response under lateral forces, such as those caused by seismic activity. As depicted in **Figure 11**, the research applies this methodology to both structural designs. **Figure 11a** illustrates the specific load paths used for analyzing the Piloti-type RC structure, which features unique open spaces on the ground floor. In contrast, **Figure 11b** shows the load directions applied to the non-Piloti-type RC structure, which has a more conventional design with reinforced walls throughout. Analyzing both structures under the same two load directions ensures a consistent comparison of their performance under nonlinear conditions. The analysis is executed using a displacement control system, with control implemented through conjugate displacement. The pushover analysis consists of a planned sequence of 100 analytical steps, and each step is structured to account for varying displacement levels, enabling a detailed assessment of the structural response as lateral loads progressively increase. This multi-step approach provides a comprehensive understanding of the structural behavior, capturing critical data points that reveal how deformations evolve under load and identifying key moments in the load-displacement relationship [12–14,17]. The 100-step framework ensures a thorough investigation of the structural performance, offering insights into its overall stability and resilience.

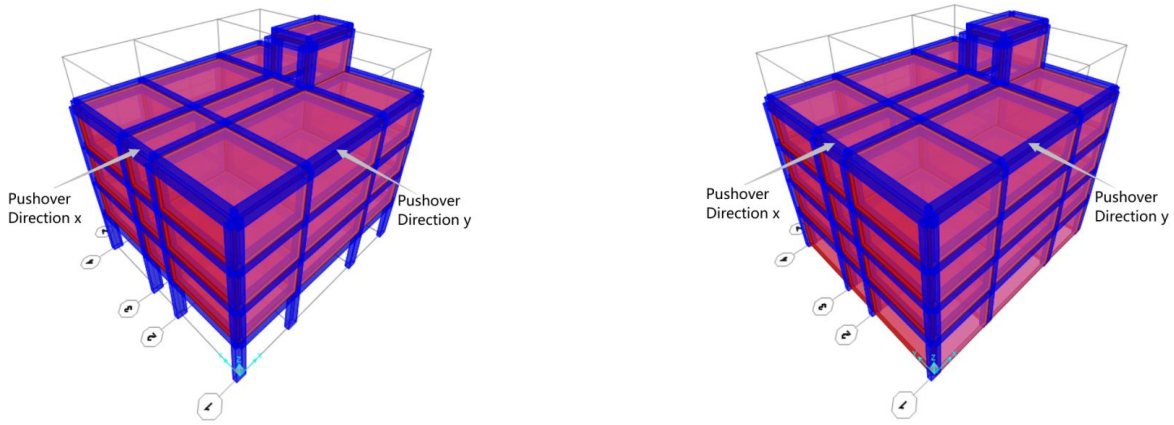

(a) **(b)**

Figure 11. Nonlinear pushover analysis. **(a)** Piloti-type RC structure; **(b)** non-Piloti-type RC structure.

3. Discussion of nonlinear pushover analysis

3.1. Performance point

This research provides a comprehensive presentation of essential results, as displayed in **Tables 6–9**, offering a thorough comparison of the performance points for both the Piloti-type and non-Piloti-type RC structures. These tables summarize key structural performance characteristics based on two different evaluation criteria (ACT-40 and FEMA 440) used in the nonlinear pushover analysis. By presenting these critical data points, the tables highlight the fundamental differences between the two structural designs, offering insights into how each behaves under the applied seismic loads. The results encapsulated in these tables serve as a crucial component of this research, allowing for a deeper understanding of the distinct dynamic responses and structural resilience of the Piloti-type and non-Piloti-type RC structures.

The performance points presented in **Tables 6** and **7** are derived from the analytical results based on ACT-40, focusing on the *x* and *y* directions of analysis. To further enrich these findings, **Tables 8** and **9** provide additional insights specifically aimed at assessing seismic performance based on FEMA 440. Due to this, the data from these tables offer a robust evaluation framework, aligning the research with industry standards for seismic performance. The integration of both ACT-40 and FEMA 440 ensures that the analysis is comprehensive, following established guidelines to evaluate the structural behavior under seismic loads, and delivering a well-rounded assessment of the resilience of the two RC structures.

Based on the guidelines provided in KDS 41 17 00: 2022, calculating the spectral accelerations for the 1-second and 0.2-second periods is essential for assessing the performance points of the structure, and the calculation equations of S_{D1} (1-sec spectral accelerations) and S_{DS} (0.2-sec spectral accelerations) are illustrated below:

$$S_{D1} = S \times F_V \times \frac{2}{3} \tag{2}$$

$$S_{DS} = S \times 2.5 \times F_a \times \frac{2}{3} \tag{3}$$

where S represents the effective ground acceleration value for a 2400-year return period earthquake, as referenced in KDS 41 17 00: 2022. Additionally, referring to Tables 4.2-1 and 4.2-2 according to KDS 41 17 00: 2022, the factors F_a and F_v denote the acceleration-based site coefficient and velocity-based site coefficient respectively.

In this research, the seismic performance of the Piloti-type and non-Piloti-type RC structure is evaluated based on its location and the criteria set out in KDS 41 17 00: 2022. The analysis incorporates site-specific conditions, classified as site-class S4, with a long period of 8 seconds. Using Equations (2) and (3), the spectral accelerations of S_{D1} and S_{DS} can be computed. The value of S_{D1} is found to be 1 g, indicating the acceleration of the structure during a 1-second period, while S_{DS} is calculated as 0.4 g, representing the acceleration over a shorter 0.2-second period.

According to **Table 6**, the nonlinear pushover analysis results for performance points under ACT-40 reveal that the Piloti-type RC structure exhibits a significantly higher base shear in the *x* direction compared to the non-Piloti-type RC structure.

Specifically, the base shear for the Piloti-type RC structure is 6568.37 kN, while the non-Piloti-type RC structure shows a lower value of 3669.58 kN, indicating that the base shear of the Piloti-type structure is approximately 44% larger. This higher base shear also leads to a longer lateral displacement for the Piloti-type RC structure, measuring 1.87 mm in the *x* direction, compared to just 0.39 mm for the non-Piloti-type structure. This represents a 79% increase in lateral displacement, highlighting the Piloti-type RC structure's more significant dynamic response and its inherent structural weakness under seismic loading in the *x* direction.

Table 6. Performance point—Direction *x* (ACT-40).

Type	Base Shear	Displacment	S_a	S_d	Teff	Beff
	kN	mm	g	mm	Period	-
Piloti	6568.37	1.87	0.50	1.68	0.12	0.05
non-Piloti	3669.58	0.39	0.33	0.20	0.05	0.05

Table 7. Performance point—Direction *y* (ACT-40).

Type	Base Shear	Displacment	S_a	S_d	Teff	Beff
	kN	mm	g	mm	Period	-
Piloti	4212.45	5.35	0.50	4.17	0.18	0.05
non-Piloti	3795.47	0.47	0.34	0.25	0.05	0.05

In the *y* direction, similar comparative results are observed, as illustrated in **Table 7**. The Piloti-type RC structure exhibits a 10% larger base shear compared to the non-Piloti-type RC structure. Additionally, the Piloti-type RC structure shows a significantly longer structural lateral displacement, with an increase of 91% in the *y* direction. These findings further highlight the more pronounced dynamic response of the Piloti-type structure and emphasize the increased potential vulnerabilities of its design under seismic loading in the *y* direction.

The analytical results for S_a (spectral acceleration) and S_d (spectral displacement) further reinforce the findings related to base shear and structural lateral displacement. As shown in **Table 6**, in the *x* direction, the Piloti-type RC structure exhibits a 34% faster S_a compared to the non-Piloti-type RC structure. Additionally, the Piloti-type structure demonstrates a much longer S_d, approximately 88% greater than that of the non-Piloti-type structure. The analysis through direction *x* also reveals that the Piloti-type RC structure has a longer structural period, which indicates greater structural flexibility but also points to potential weaknesses when compared to the non-Piloti-type structure. The longer structural period is essential for understanding how the Piloti-type structure responds to seismic forces, highlighting areas that may require additional reinforcement or careful consideration during the design process to improve its overall stability.

Focusing on the analytical results in the *y* direction, as presented in **Table 7**, similar comparative findings emerge. The Piloti-type RC structure exhibits a 32% faster S_a and a significantly longer S_d, approximately 94% greater than that of the non-Piloti-type structure. Additionally, the structural period of the Piloti-type RC structure is about 71% longer than the non-Piloti-type structure. These findings in the *y* direction

further reinforce the results observed in the *x* direction, emphasizing that while the Piloti-type RC structure demonstrates increased flexibility, it also shows potential structural weaknesses compared to the non-Piloti-type structure.

Table 8. Performance point—Direction *x* (FEMA 440).

Type	Base Shear	Displacment	S_a	S_d	Teff	Ducitility	Beff	M
	kN	mm	g	mm	Period	-	-	-
Piloti	6568.37	1.19	0.50	1.68	0.12	1.00	0.05	1.00
non-Piloti	3669.58	0.39	0.33	0.20	0.05	1.00	0.05	1.00

Table 9. Performance point—Direction *y* (FEMA 440).

Type	Base Shear	Displacment	S_a	S_d	Teff	Ducitility	Beff	M
	kN	mm	g	mm	Period	-	-	-
Piloti	4212.45	5.35	0.50	4.17	0.18	1.00	0.05	1.00
non-Piloti	3795.47	0.47	0.34	0.25	0.05	1.00	0.05	1.00

To further enhance the understanding of the performance points, **Tables 8** and **9** present the nonlinear pushover analysis results using FEMA 440, examining the *x* and *y* directions. These results affirm that the Piloti-type RC structure exhibits several key characteristics, including a larger base shear, longer structural lateral displacement, faster S_a, longer S_d, and a longer structural period. Similar to the findings from the ACT-40 analysis, the results from FEMA 440 also underscore the potential structural vulnerabilities of the Piloti-type RC structure when compared to the non-Piloti-type RC structure. Including the results of base shear, structural lateral displacement, S_a, and S_d, the longer structural period also indicates that the Piloti-type design may be more susceptible to weaknesses, especially under external forces like seismic activity.

3.2. Capacity curve

In the context of nonlinear pushover analysis, a capacity curve represents the relationship between base shear and structural lateral displacement as the structure is subjected to increasing lateral loads. The curve typically plots base shear, which is the total horizontal force at the base of the structure, against roof displacement, or the horizontal movement at the top of the structure. This graphical representation helps in understanding how the structure responds to lateral forces, such as those induced by earthquakes. Unlike linear analysis, which assumes the structure behaves elastically, the capacity curve captures the nonlinear behavior of the structure, including key aspects such as yielding and plastic deformations. This makes it a critical tool for assessing how the structure performs under severe loading conditions. According to research by Shah and Patel [25], the capacity curve also helps identify various performance levels of the structure, such as IO (immediate occupancy), LS (life safety), and CP (collapse prevention). These points on the curve indicate the levels of damage the structure can withstand before reaching a critical state, making the capacity curve essential for understanding the structural response under extreme conditions.

In this research, **Figure 12** presents the capacity curves for both the Piloti-type and non-Piloti-type RC structures. **Figure 12a** illustrates the capacity curves in the *x* direction, while **Figure 12b** shows the results in the *y* direction. According to **Figure 12a**, the non-Piloti-type RC structure demonstrates a significantly higher base shear compared to the Piloti-type RC structure in the *x* direction. On the other hand, the Piloti-type RC structure exhibits a longer structural lateral displacement. Similarly, **Figure 12b** reveals the same trend in the *y* direction, with the non-Piloti-type RC structure showing a larger base shear, while the Piloti-type structure continues to appear with a longer lateral displacement. The analytical results from both directions emphasize the potential structural weaknesses of the Piloti-type RC structure, as its lower base shear combined with a longer lateral displacement suggests greater flexibility, which could pose structural damages under seismic loads.

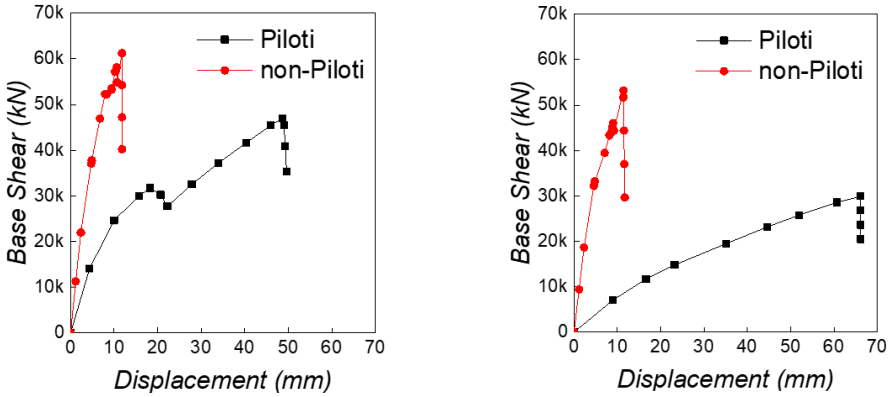

Figure 12. Capacity curves. **(a)** Direction *x*; **(b)** Direction *y*.

To further enrich the findings from the capacity curves, the analysis of the slope within the structural elastic zone reinforces the discussion. As shown in **Table 10**, the Piloti-type RC structure demonstrates a lower slope value in the elastic zone compared to the non-Piloti-type RC structure in both the *x* and *y* directions. In the *x* direction, the non-Piloti-type RC structure shows a slope value that is 66.06% larger than that of the Piloti-type structure, while in the *y* direction, the difference is even more pronounced, with the non-Piloti-type structure exhibiting a 90.42% larger slope value. These results emphasize the higher stiffness of the non-Piloti-type RC structure, highlighting its superior structural performance in the elastic zone. However, the lower slope of the Piloti-type structure suggests potential structural weakness, particularly when subjected to external forces such as seismic activity, where its reduced stiffness may lead to greater vulnerability.

Table 10. Slope of the elastic zone.

Direciton-*x*		**Direciton-*y***	
Piloti	non-Piloti	Piloti	non-Piloti
3239.73	9544.83	787.41	8217.01

When assessing the seismic performance of the structure, the capacity spectrum method plays a crucial role in determining the structural performance level. This

method involves establishing a target displacement, which serves as a reference point for evaluating how the structure will behave under seismic conditions. It then conducts a graphical comparison between the structural capacity and the seismic demand, allowing for a clear visualization of how the structure responds to seismic forces. One of the key features of the capacity spectrum method is its ability to visually represent both the structural capacity and the expected performance under seismic stress, providing an insightful understanding of the seismic resilience and overall behavior under earthquake loading conditions.

As referenced by Hakim [26], the calculation of the capacity spectrum relies on the relationship between two fundamental parameters S_a (spectral acceleration) and S_d (spectral displacement). These parameters are crucial for understanding how a structure will respond to seismic forces, and their relationship is expressed in the equations provided below:

$$\frac{S_a}{g} = \frac{V_b}{w} \times \frac{1}{a} \tag{4}$$

where V_b is base shear force, w is building load weight, and a is the modal mass coefficient.

$$S_d = \frac{T^2 S_a}{4\pi^2} \tag{5}$$

where T is the structural period, and S_a is the spectral acceleration that can be calculated through the equation above.

By connecting S_a and S_d, this approach offers deeper insights into the structural seismic performance and is key in determining how it behaves under varying levels of earthquake-induced stress. This method forms the basis for calculating capacity spectra, which is a critical part of performance-based seismic analysis.

Based on the analytical results from the capacity curves and using Equations (4) and (5), the capacity spectrum for both the Piloti-type and non-Piloti-type RC structures in this research is presented in **Figure 13**. **Figure 13a** illustrates the capacity spectrum for the *x* direction, while **Figure 13b** shows it for the *y* direction. Notably, both capacity spectra include a reference to the target response spectrum from KDS 41 17 00: 2022, which provides a key benchmark for evaluating the seismic performance of the structures. The inclusion of the response spectrum in the analysis allows for a more comprehensive assessment, visually comparing the structural capacity to seismic demand. This comparison is critical for understanding the dynamic behavior of the structures in the context of the specific seismic criteria outlined by KDS 41 17 00: 2022.

According to **Figure 13a**, the capacity spectrum results confirm that both the Piloti-type and non-Piloti-type RC structures satisfy the requirements of the Korean standards outlined in KDS 41 17 00: 2022 for the *x* direction. This indicates that both structures are acceptable for site-class S4 when analyzed along the *x* direction. However, a comparison of the capacity spectrum curves between the two structures reveals that the non-Piloti-type RC structure exhibits a faster S_a and a shorter S_d than the Piloti-type RC structure in this direction. These findings align with previous

discussions on the capacity curves, further reinforcing the observation that the Piloti-type structure demonstrates potential structure weakness under the external force.

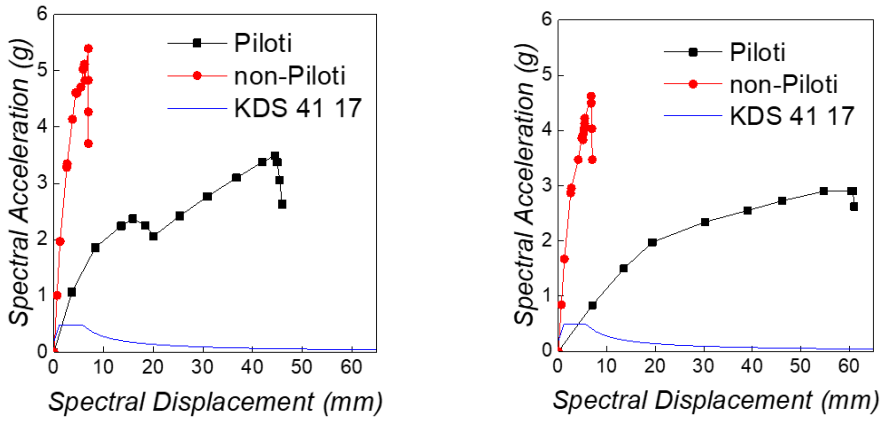

Figure 13. Capacity spectrum. **(a)** Direction *x*; **(b)** Direction *y*.

When examining the capacity spectrum results for both Piloti-type and non-Piloti-type RC structures in the *y* direction, as shown in **Figure 13b**, it is evident that both structures comply with the requirements of the Korean standard KDS 41 17 00: 2022 for site-class S4. This confirms their seismic acceptability when analyzed along the *y* direction. However, comparing the analytical results of the capacity spectrum curves for the two structures highlights similar findings to those observed in the *x* direction. Specifically, the Piloti-type RC structure exhibits a smaller S_a and a longer S_d, indicating potential structural weaknesses under external seismic forces. These results also reinforce earlier discussions about the potential structural weakness in the Piloti-type structure under seismic activities.

In discussing the capacity curves, slope values in the structural elastic zone, and the capacity spectrum, the comparison between the Piloti-type and non-Piloti-type RC structures reveals distinct differences in seismic performance based on the structural orientation. The analytical results indicate that in the *x* direction, the structures exhibit a higher base shear, shorter lateral displacement, larger slope in the elastic zone, faster S_a, and shorter S_d compared to the *y* direction. This phenomenon can be explained by the specific structural design, where the longer side (14,800 mm) of the structure is aligned with the *x* direction, while the shorter side (13,000 mm) is aligned with the *y* direction. The increased length in the *x* direction enhances the overall stiffness of the structure, which contributes to better performance under seismic loads. As a result, the length of the structure aligned with the load direction significantly influences the structural seismic behavior, emphasizing the importance of structural design in nonlinear pushover analysis.

3.3. Layer displacement and drift ratio

The evaluation of plastic hinge states plays a critical role in understanding the performance of structures under nonlinear pushover analysis. The research by Eslami and Ronagh [27] emphasizes the importance of analyzing plastic hinge states in RC structures, revealing how these hinges affect the overall structural behavior, especially during seismic events. Eslami and Ronagh [27] indicate that the formation and

progression of plastic hinges are key to determining the structural ability to absorb and redistribute forces, making it essential for understanding potential failure mechanisms. In parallel, the research conducted by Damcı et al. [28] focuses on plastic hinge analysis in 3D frame structures, demonstrating the importance of this analysis within the context of static pushover procedures. Their findings confirm that a thorough understanding of plastic hinge behavior is essential for accurately assessing the resilience, strength, and integrity of structures when subjected to increasing lateral loads.

In this research, the analysis of layer displacement is focused on the plastic hinge state known as C (collapse prevention), which marks the critical point where the structure transitions from the elastic to the plastic region and approaches the onset of collapse. The plastic hinge state C represents the moment when the structure experiences significant deformation, indicating that it is nearing its failure limit. As illustrated in **Figure 14**, the behavior of both the Piloti-type and non-Piloti-type RC structures is captured when their plastic hinges reach the C state. **Figure 14** provide a detailed visualization of how the structures respond in both the *x* and *y* analytical directions under this critical condition. These results are crucial for understanding how each structure approaches collapse, offering insights into their capacity to withstand extreme seismic loads and the resilience of the designs in preventing total structural failure. By focusing on the C state, this research highlights the importance of tracking plastic hinge development as a key factor in evaluating the ultimate performance and safety of RC structures.

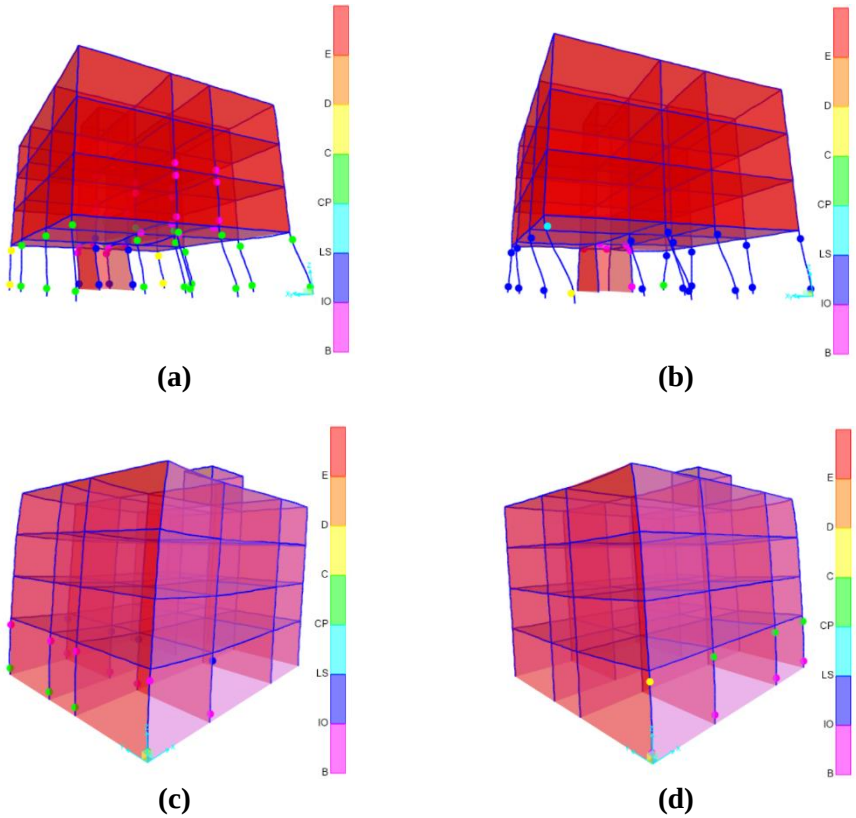

Figure 14. Structural deformations. **(a)** Direction *x* (Piloti); **(b)** Direction *y* (Piloti); **(c)** Direction *x* (non-Piloti); **(d)** Direction *y* (non-Piloti).

The structural lateral displacement of both Piloti-type and non-Piloti-type RC structures is assessed based on their deformation when the plastic hinge reaches the critical C state, indicating collapse prevention. This stage marks the point where the structures begin to undergo significant plastic deformation, nearing failure. As shown in **Figure 15**, these displacements are plotted for both the *x* and *y* analytical directions, providing a clear comparison between the two types of RC structures. In **Figure 15a**, the lateral displacement for both structures along the *x* direction is presented, offering insight into their respective lateral responses under nonlinear pushover analysis. Meanwhile, **Figure 15b** demonstrates the structural displacements aligned with the *y* direction, further enriching the comparative analysis. The figures underscore the dynamic response of each structure as it approaches collapse, reflecting the influence of design characteristics on the ability to withstand lateral forces and highlighting critical differences in their behavior under extreme conditions.

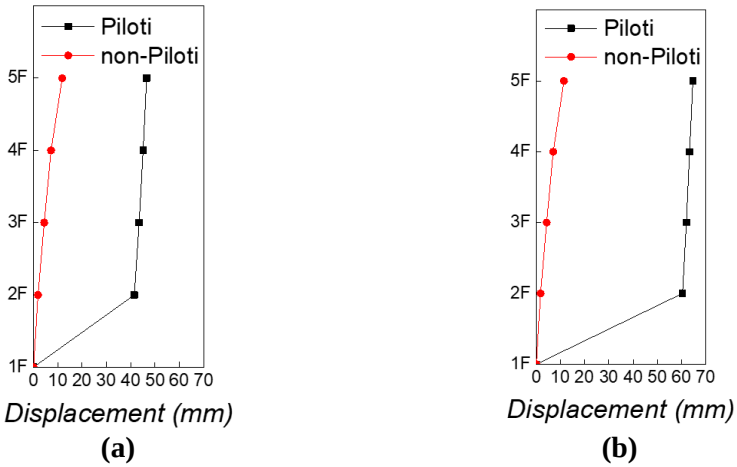

Figure 15. Layer displacement. **(a)** Direction *x*; **(b)** Direction *y*.

In the analysis of layer displacements in the *x* direction, as depicted in **Figure 15a**, the Piloti-type RC structure clearly exhibits a considerably longer layer displacement compared to its non-Piloti-type counterpart. This notable difference can be attributed to the unique architectural design of the Piloti-type structure, which features open spaces beneath the building. These open areas result in the absence of reinforced walls that typically provide resistance against external forces. Consequently, when subjected to lateral loads, the Piloti-type structure experiences extreme shear forces and moments, leading to significantly increased layer displacements. In contrast to the behavior observed in Piloti-type RC structures, the non-Piloti-type RC structures demonstrate a more progressive increase in structural lateral displacement as the number of stories increases. This gradual rise in displacement indicates a more uniform distribution of stress throughout the entire height of the structure, reflecting a consistent transmission of lateral loads across all stories. However, the Piloti-type RC structures exhibit a different response. Beyond the second floor, there is little to no change in the structural lateral displacement, which suggests that the upper portions of the building are largely disconnected from the primary mechanisms of load transmission. This phenomenon can be attributed to the extreme stress concentrations in the open spaces beneath the structure. When averaged

across both types of structures, the layer displacement in the Piloti-type design is found to be 10.61 times greater than that of the non-Piloti-type structure. This stark contrast underscores the implications of structural design on performance under seismic loading, highlighting potential vulnerabilities in the Piloti-type configuration that indicate strengthening these open spaces beneath the structures could be crucial for improving the building's overall seismic resilience.

When analyzing the layer displacement results in the analytical direction *y*, as illustrated in **Figure 15b**, a similar trend emerges, mirroring the behavior seen in the direction *x*. The Piloti-type structure consistently exhibits longer structural lateral displacements at every story when compared to the non-Piloti-type structure, as the average layer displacement in the Piloti-type design is found to be 15.79 times greater than that of the non-Piloti-type structure. This significant displacement is largely due to the absence of reinforced walls in the open spaces on the first floor of the Piloti-type structure. The lack of reinforced walls results in excessive shear forces and moments being concentrated at the ground level. As a result, the first floor effectively becomes disconnected from the rest of the structure, leading to a separation between the structural behavior of the first floor and that of the upper floors (second to fifth). This division weakens the structural integrity of the building, particularly as the upper stories (containing a substantial mass) exacerbate the stress on the already compromised first floor. The heavy mass of these upper floors aggravates the potential for structural failure under lateral forces, such as those generated by seismic activity. The analysis in the *y* direction reinforces the conclusion that the open space design of the Piloti-type structure introduces significant vulnerabilities, especially on the first floor, which may require enhanced structural reinforcement to mitigate these weaknesses.

When comparing the analytical results for layer displacement in both the *x* and *y* directions, as shown in **Figure 15a**,**b**, it is evident that the *y* direction exhibits longer layer displacements than the *x* direction for both the Piloti-type and non-Piloti-type structures. This observation underscores the significant influence that the structure design has on seismic performance. Specifically, the *x* direction, with a longer side of 14,800 mm, offers greater stiffness compared to the shorter 13,000 mm side aligned with the *y* direction. The increased structural length in the *x* direction enhances the overall stiffness of the structure, which reduces the extent of lateral displacements under seismic loading. This improved stiffness leads to better performance during seismic events, as the structure is more capable of resisting lateral forces without experiencing significant deformation. Conversely, the shorter length in the *y* direction results in less stiffness, which is reflected in the longer displacements observed in the layer analysis.

According to the previous research conducted by Peng et al. [29], the layer drift ratio is a critical metric in assessing structural performance during nonlinear pushover analysis. The layer drift ratio provides insight into how much the individual stories of the structure drift or displace horizontally relative to one another, which is particularly important when analyzing the behavior of the structure under seismic forces. Furthermore, the research by Shi et al. [9] offer a detailed methodology for calculating the layer drift ratio. The calculation relies on two key parameters: the structural lateral displacement and the height of each story as the equations illustrate below:

$$\Delta = \delta_x - \delta_{x-1} \tag{6}$$

$$\Delta_{ratio} = \frac{\Delta}{h} \tag{7}$$

where δ_x is the displacement at the *x* floor, δ_{x-1} is the displacement at the $x-1$ floor, Δ is the drift between the *x* floor and the $x-1$ floor, h is the height of the story, and Δ_{ratio} is the drift ratio.

Based on the analytical results of the layer displacement, the layer drift ratio for both the Piloti-type and non-Piloti-type RC structures are enabled to be calculated for both the *x* and *y* analytical directions. These calculations were carried out using the formulas provided in Equations (6) and (7), which take into account the structural lateral displacement and story height to derive the layer drift ratio.

As illustrated in **Figure 16**, the results offer a detailed comparison of how both structure types perform under different loading conditions in each direction. By calculating the layer drift ratio, this research provides crucial insight into the degree of horizontal movement each story undergoes relative to its height. This analysis is essential for understanding how the Piloti-type structure, with its open first-floor design, compares to the non-Piloti-type structure in terms of seismic resilience. The graphical representation of the drift ratios in **Figure 16** further underscores the variations between the two designs, highlighting areas of potential concern and structural weaknesses, particularly in the Piloti-type RC structure.

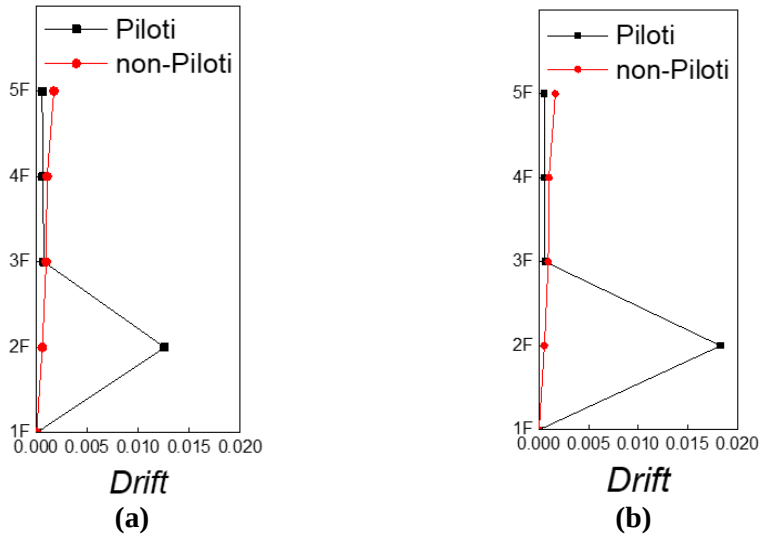

Figure 16. Layer drift ratio. **(a)** Direction *x*; **(b)** Direction *y*.

The layer drift of both Piloti-type and non-Piloti-type RC structures, as shown in **Figure 16a** for the analytical direction *x*, clearly highlights the differences in behavior between the two structural designs. For the Piloti-type structure, the most significant layer drift ratio is observed on the second floor, where the open spaces underneath the structure have a pronounced impact. After the second story, there is relatively little change in the layer drift ratio for the upper stories (second to fifth), suggesting that much of the lateral deformation is concentrated on the first floor, the open spaces underneath the structure. In contrast, the non-Piloti-type structure exhibits a more

gradual and slight increase in the layer drift ratio as the building height increases, showing a more uniform distribution of lateral displacement throughout the stories. This gradual increase aligns with the non-Piloti-type structural design, which provides more consistent stiffness and resistance to lateral loads across all floors. The analytical results in the *x* direction emphasize the structural vulnerability of the Piloti-type design, particularly on the second floor, where the layer drift ratio is 22.39 times greater than that of the non-Piloti-type structure. This stark difference underscores the potential weaknesses in the Piloti-type structure, especially on the first floor with the open space, which is more susceptible to extreme deformation under seismic forces.

The analytical results for the layer drift ratio in the *y* direction, as illustrated in **Figure 16b**, present a similar phenomenon to what was observed in the *x* direction. Specifically, the second story of the Piloti-type structure demonstrates a significantly larger layer drift ratio compared to the non-Piloti-type structure, reflecting the discussion about the structural performance of the Piloti-type design in the *x* direction. In the *y* direction, the layer drift ratio for the Piloti-type structure is 33.69 times greater than that of the non-Piloti-type structure in the second story, and this substantial difference also highlights the pronounced concentration of deformation on the first floor for the Piloti-type design in the *y* direction. The presence of open spaces on the first floor of the Piloti-type structure contributes to this imbalance, as the lack of reinforced walls leaves the structure more vulnerable to external lateral forces. Without adequate resistance at the lower levels, the upper stories experience a disproportionate amount of movement, further exacerbating the structural weaknesses under seismic conditions.

These results emphasize that the Piloti-type structure is not only susceptible to extreme deformations in the *x* direction but also in the *y* direction. The vulnerability due to the open first floor is a significant factor in both directions, underscoring the need for targeted reinforcement to improve the structural resilience of the Piloti-type design when subjected to external lateral forces.

In the analysis of layer displacement for both Piloti-type and non-Piloti-type RC structures, the comparison between the *x* and *y* directions reveals that the layer drift ratio is consistently larger in the *y* direction. This phenomenon highlights the influence of the structural design on seismic performance. Specifically, the longer side of the RC structure, measuring 14,800 mm and aligned with the *x* direction, contributes to the overall stiffness of the structure, allowing it to better resist seismic forces in that direction. The shorter dimension of 13,000 mm aligned with the *y* direction, however, offers less structural stiffness, which leads to a higher layer drift ratio under seismic loads. This difference between the two directions emphasizes the importance of the building's geometric configuration in determining its seismic behavior.

The increased length along the *x* direction not only enhances the stiffness but also reduces the structural deformations under external forces, resulting in better performance during seismic events. In contrast, the *y* direction, with its shorter span, exhibits greater deformation and a larger layer drift ratio, indicating that structures with similar geometric proportions might require additional reinforcement along the shorter axis to improve overall seismic resilience.

4. Conclusion

In contemporary urban environments, the increasing demand for living space has necessitated innovative structural designs. The Piloti-type RC structure has become a popular solution to address urban space issues [30–32]. This structural design creates a more flexible and dynamic urban atmosphere compared to traditional building designs, aligning with the growing population in metropolitan cities where optimizing living space is crucial. Despite its advantages, the Piloti-type RC structure presents significant structural challenges, particularly due to the absence of reinforced walls on the open ground floor. This absence creates a potential structural weakness, leaving the building more vulnerable to collapse during seismic events. This vulnerability was starkly highlighted during the 2017 Pohang earthquake, which caused significant damage to Piloti-type structures due to their reduced seismic resistance. To address these concerns, this research investigates the differences between Piloti-type and non-Piloti-type RC structures under nonlinear pushover analysis, offering valuable insights into their behavior under seismic forces. The analytical results of this research, derived through nonlinear pushover analysis in SAP 2000, are cross-validated by referencing previous research [33–35]. As Xia et al. [34] and Xia et al. [35] illustrate, the analytical results not only affirm the reliability and accuracy of the analytical approach employed in this research but also supply critical data on the nonlinear properties of materials such as concrete and rebar. By aligning with previous studies, this research strengthens the credibility of its findings, confirming that SAP 2000 provides robust results for nonlinear structural analysis. By thoroughly analyzing these differences, this study aims to provide a meaningful reference for structural reinforcement of Piloti-type designs, ensuring their resilience in future urban developments.

(1) The comparative analysis of performance points for both Piloti-type and non-Piloti-type RC structures reveals significant differences in the structural behavior under nonlinear pushover analysis. The findings clearly indicate that non-Piloti-type structures exhibit superior performance characteristics. Specifically, these structures demonstrate smaller base shear (ACT-40_(non-Piloti-type structures: 3669.58 kN for direction *x*; 3795.47 kN for direction *y*/Piloti-type structures: 6568.37 kN for direction *x*; 4212.45 kN for direction *y*)), (FEMA 440_(non-Piloti-type structures: 3669.58 kN for direction *x*; 3795.47 kN for direction *y*/Piloti-type structures: 6568.37 kN for direction *x*; 4212.45 kN for direction *y*)), which reduces the overall lateral forces acting on the building, and shorter structural displacements (ATC-40_(non-Piloti-type structures: 0.39 mm for direction *x*; 0.47 mm for direction *y*/Piloti-type structures: 1.87 mm for direction *x*; 5.35 mm for direction *y*)), (FEMA 440_(non-Piloti-type structures: 0.39 mm for direction *x*; 0.47 mm for direction *y*/Piloti-type structures: 1.19 mm for direction *x*; 5.35 mm for direction *y*)), which indicate less deformation under load.

(2) The lower values of S_a and S_d observed in non-Piloti-type structures reflect their enhanced ability to withstand seismic forces without experiencing significant movement (ACT-40_(non-Piloti-type structures: 0.33 g and 0.2 mm for direction *x*; 0.34 g and 0.25 mm for direction *y*/Piloti-type structures: 0.5 g and 1.68 mm for direction *x*; 0.5 g and 4.17 mm for direction *y*)), (FEMA 440_(non-Piloti-type structures: 0.33 g and 0.2 mm for direction *x*; 0.34 g and 0.25 mm for direction

y/Piloti-type structures: 0.5 g and 1.68 mm for direction *x*; 0.5 g and 4.17 mm for direction *y*)). Furthermore, the shorter structural periods associated with non-Piloti-type designs suggest greater stiffness (ACT-40_(non-Piloti-type structures: 0.05 for direction *x*; 0.05 for direction *y*/Piloti-type structures: 0.12 for direction *x*; 0.18 for direction *y*)), (FEMA 440_(non-Piloti-type structures: 0.05 for direction *x*; 0.05 for direction *y*/Piloti-type structures: 0.12 for direction *x*; 0.18 for direction *y*)), which is crucial for stability during seismic events. In contrast, the Piloti-type structures show heightened vulnerability, as their design flaws become apparent under seismic activities, emphasizing their potential structural weaknesses.

(3) The examination of capacity curves and capacity spectra has provided crucial insights that bolster the findings related to performance points in the analysis of Piloti-type RC structures. Specifically, the discussions reveal significant structural vulnerabilities inherent in the design of Piloti-type structures, particularly due to the open space configuration on the first floor. The absence of reinforced walls in the open areas exposes the structure to extreme shear forces during seismic activities, leading to potentially catastrophic damage. When subjected to seismic forces, the lack of adequate reinforced walls can result in excessive lateral movement and stress concentration, ultimately causing structural failure.

(4) The layer drift ratio which quantifies how much each story of the structure moves relative to the others, highlights the critical issues due to the Piloti-type structures. In Piloti-type structures, the drift ratio indicates significant deformation (non-Piloti-type structures: 0.0017 for direction *x*; 0.0016 for direction *y*/Piloti-type structures: 0.0126 for direction *x*; 0.0183 for direction *y*), suggesting that the open space design not only compromises the integrity of the structure but also makes it more susceptible to damage during seismic activities.

The comparative analysis of Piloti-type and non-Piloti-type RC structures through nonlinear pushover analysis reveals critical differences in their structural performance. While Piloti-type structures bring several advantages to modern urban living, the research emphasizes that the associated structural issues must not be overlooked, particularly the open space design on the first floor, which poses significant risks, potentially resulting in devastating human and financial losses during seismic events. The nonlinear pushover analysis clearly identifies the vulnerabilities of Piloti-type RC structures, especially regarding the ability to withstand lateral forces. The lack of reinforced walls in the open areas contributes to increased deformation and shear forces, leading to an elevated risk of structural failure. These findings are not just theoretical but also reflect real-world implications, underscoring the necessity for rigorous assessment and design improvements. This research aims to serve as a vital reference for future research focused on reinforcing Piloti-type structures, especially concerning open space configurations. Due to this, this research is expected to advance the design of Piloti-type RC structures and provide a reference for the reinforcement of the structure to ensure structural safety under seismic damage.

Author contributions: Conceptualization, MS; methodology, MS; software, MS; validation, MS and MC; formal analysis, MS; investigation, MS; resources, MS; data

curation, MS; writing—original draft preparation, MS; writing—review and editing, MS; visualization, MS; supervision, MS and YC; project administration, MS; funding acquisition, MS. All authors have read and agreed to the published version of the manuscript.

Conflict of interest: The authors declare no conflict of interest.

References

1. Shin J, Choi I, Kim J. Rapid decision-making tool of Piloti-type RC building structure for seismic performance evaluation and retrofit strategy using multi-dimensional structural parameter surfaces. Soil Dynamics and Earthquake Engineering. 2021; 151: 106978.
2. Honda T, Omata T, Oda Y, et al. A study on characteristics of the tsunami force acting on members of piloti-type structures. Journal of Japan Society of Civil Engineers Ser B3 (Ocean Engineering). 2021; 73(2): 96–101.
3. Hwang KR, Lee HS. Seismic damage to RC low-rise building structures having irregularities at the ground story during the 15 November 2017 Pohang, Korea, Earthquake. Journal of the Earthquake Engineering Society of Korea. 2018; 22(3): 103–111.
4. Kim T, Park JH, Yu E. Seismic fragility of low-rise piloti buildings based on 2017 Pohang earthquake damage. Journal of Building Engineering. 2023; 76: 107032.
5. Kang S, Kim B, Bae S, et al. Earthquake-induced ground deformations in the low-seismicity region: A case of the 2017 M5. 4 Pohang, South Korea, earthquake. Earthquake Spectra. 2019; 35(3): 1235–1260.
6. Dang-Vu H, Lee DH, Shin J, et al. Influence of shear-axial force interaction on the seismic performance of a piloti building subjected to the 2017 earthquake in Pohang Korea. Structural Concrete. 2020; 21(1): 220–234.
7. Kim T, Chu Y, Kim SR, et al. Seismic behavior of domestic piloti-type buildings damaged by 2017 Pohang earthquake. Journal of the Earthquake Engineering Society of Korea. 2018; 22(3): 161–168.
8. Kim B, Ji Y, Kim M, et al. Building damage caused by the 2017 M5. 4 Pohang, South Korea, earthquake, and effects of ground conditions. Journal of earthquake engineering. 2022; 26(6): 3054–3072.
9. Shi M, Xu X, Choi Y. Nonlinear Pushover Analysis of the Influences on RC Footing for the External Elevator Well. Open Journal of Applied Sciences. 2024; 14(7): 1823–1842.
10. Bhandari M, Bharti SD, Shrimali MK, et al. Assessment of proposed lateral load patterns in pushover analysis for base-isolated frames. Engineering Structures. 2018; 175: 531–548.
11. Shayanfar MA, Ashoory M, Bakhshpoori T, et al. Optimization of modal load pattern for pushover analysis of building structures. Structural Engineering and Mechanics. 2013; 47(1): 119–129.
12. Jalilkhani M, Ghasemi SH, Danesh M. (2020). A multi-mode adaptive pushover analysis procedure for estimating the seismic demands of RC moment-resisting frames. Engineering Structures, 213, 110528.
13. Dorri F, Ghasemi H, Nowak A. Developing a lateral load pattern for pushover analysis of EBF system. Reliability Engineering and Resilience. 2019; 1(1): 42–54.
14. Pierre AJ, Hidayat I. Seismic performance of reinforced concrete structures with pushover analysis. IOP Conference Series: Earth and Environmental Science. 2020; 426(1): 012045.
15. Faal HN, Poursha M. Applicability of the N2, extended N2 and modal pushover analysis methods for the seismic evaluation of base-isolated building frames with lead rubber bearings (LRBs). Soil Dynamics and Earthquake Engineering. 2017; 98: 84–100.
16. Ismaeil M. Seismic capacity assessment of existing RC building by using pushover analysis. Civil Engineering Journal. 2018; 4(9): 2034–2043.
17. Shamivand A, Akbari J, Allahyari P. An analytical formulation to extract the capacity curve of steel structures. Asian Journal of Civil Engineering. 2022; 23(7): 1183–1195.
18. Ismaeil M, Sobaih M, Akl A. Seismic capacity assessment of existing RC buildings in the Sudan by using pushover analysis. Open Journal of Civil Engineering. 2015; 5(2): 154–174.
19. Harris J, Speicher M. Assessment of performance-based seismic design methods in ASCE 41 for new steel buildings: Special moment frames. Earthquake Spectra. 2018; 34(3): 977–999.

20. Sujayakumar DS, Venkatesh SV, Mithanthaya IR. The Behaviour of Hinges in Buildings Over Various Monitored Displacement-Pushover Analysis. International Journal of Emerging Engineering and Technology. 2022; 1(2): 13–18.
21. Han SW, Lee CS, Paz Zambrana MA, et al. Calibration factor for ASCE 41–17 modeling parameters for stocky rectangular RC columns. Applied Sciences. 2019; 9(23): 5193.
22. Choi KK, Kim JC. Seismic Capacity of RC Structures with Non-seismic Details and Standard Details for Structural Retrofit. Magazine of the Korea Concrete Institute. 2015; 27(6): 31–35.
23. Al Mamuna A, Saatcioglu M. Analytical modeling of moderately ductile RC frame structures for seismic performance evaluation using PERFORM-3D. Earthquake Spectra. 2019; 35(2): 635–652.
24. Masrilayanti M, Hasibuan YA, Kurniawan R, et al. Performance evaluation of high-rise apartment building using pushover analysis. In: E3S Web of Conferences. EDP Sciences; 2023. Volume 429. p. 05024.
25. Shah MA, Patel NK. Pushover Analysis: Recent State of Art. In: Sustainable Building Materials and Construction: Select Proceedings of ICSBMC 2021. Springer Nature; 2022. pp. 241–246.
26. Hakim RA. Seismic assessment of RC building using pushover analysis. International journal of engineering science and technology. 2013; 1: 72–77.
27. Eslami A, Ronagh HR. Effect of elaborate plastic hinge definition on the pushover analysis of reinforced concrete buildings. The Structural Design of Tall and Special Buildings. 2014; 23(4): 254–271.
28. Damcı E, Öztorun NK, Çelik T. A plastic hinge method for static pushover analysis of 3D frame structures. Australian Journal of Structural Engineering. 2024; 25(4): 1–22.
29. Peng WJ, Li ZA, Tao MX. Evaluation and story drift ratio limits of structures with separated gravity-and lateral-load-resisting systems using pushover analysis. Journal of Building Engineering. 2023; 76: 107223.
30. Li J, Shan X, Deng Q. Study on the Impact of Design Factors of Piloti Forms on the Thermal Environment in Residential Quarters. Buildings. 2024; 14(5): 1303.
31. Lee JE, Yoon YH. Influences of the residential environment on the apartment remodeling: involving the expansion of households and dwelling area. LHI Journal of Land, Housing, and Urban Affairs. 2011; 2(3): 259–268.
32. Xi TY, Ding JH, Jin H. Study on the Influence of Piloti Arrangement on Outdoor Wind Environment in Residential Blocks in Subtropical Climate Zones. Applied Mechanics and Materials. 2017; 858: 227–233.
33. Xia H, Sun Q, Wang S. Influence of strain rate effect on energy absorption characteristics of bio-inspired honeycomb column thin-walled structure under impact loading. Case Studies in Construction Materials. 2023; 18: e01761.
34. Xia H, Sun Q, Wang S. FE model to define impacting resistance behavior of RC beams protected by AlSi10Mg buffer interlayer. In: Structures. Elsevier; 2023. Volume 58. p. 105329.
35. Xia H, Fang X, Yu Q, et al. The impact protection behavior of UHPC composite structure on RC columns. Case Studies in Construction Materials. 2024; 21: e03866.